nature communications

Article

https://doi.org/10.1038/s41467-025-63701-x

Spin density wave rather than tetragonal structure is prerequisite for superconductivity in $La_3Ni_2O_{7-\delta}$

Received: 13 January 2025

Accepted: 26 August 2025

Published online: 15 October 2025

Check for updates

Mengzhu Shi[1,2,9], Di Peng[3,4,9], Yikang Li[1,2], Shaohua Yang[5], Zhenfang Xing[4], Yuzhu Wang[6], Kaibao Fan[1,2], Houpu Li[1,2], Rongqi Wu[1,2], Binghui Ge[5], Zhidan Zeng[4], Qiaoshi Zeng[3,4], Jianjun Ying[1,7], Tao Wu[1,2,7,8] ✉ & Xianhui Chen[1,2,7,8] ✉

The pressure-induced high-temperature (T_c) superconductivity in nickelates $La_3Ni_2O_{7-\delta}$ has sparked significant interest to explore its superconductivity at ambient pressure. Whether the pressure-stabilized tetragonal structure is a prerequisite for achieving nickelate superconductivity at ambient pressure is under hot debate. Here, by post-annealing in high oxygen pressure environment, tetragonal $La_3Ni_2O_{6.92}$ single crystals are successfully obtained at ambient pressure, which exhibits a metallic behavior without a SDW transition. Moreover, superconductivity is also absent at high pressures up to ~ 70 GPa. Furthermore, by utilizing Helium as the pressure medium, we found that the superconductivity in pressurized orthorhombic $La_3Ni_2O_{6.85}$ is achieved in orthorhombic structure rather than tetragonal structure claimed previously. All these findings demonstrate that tetragonal structure is not prerequisite for achieving superconductivity in $La_3Ni_2O_{7-\delta}$. Finally, our present work suggests a deep correlation between SDW order and superconductivity, which imposes stringent constraints on the underlying mechanism for pressure-induced superconductivity in nickelates.

Search for high-temperature superconductivity in nickelates has attracted a lot of interest amongst physicists and materials researchers after the discovery of cuprate superconductivity[1–7]. In 2019, the breakthrough in infinite-layer nickelate $Nd_{1-x}Sr_xNiO_2$ thin film triggered a new wave of searching for novel nickel-based superconductors[8]. Recently, the nickelate superconductor family has been successfully expanded to the Ruddlesden-Popper (RP) phases $La_{n+1}Ni_nO_{3n+1}$, with $n = 2$[9] and $n = 3$[10–13]. The superconducting transition temperature (T_c) in $La_3Ni_2O_{7-\delta}$ exceeds the liquid-nitrogen boiling temperature, suggesting a new family of high-temperature superconductors[14–26]. However, unlike the infinite-layer nickelate thin films, the realization of superconductivity in these *RP* nickelates requires extremely high-pressure conditions, which hinders most spectroscopic measurements of the superconducting state and complicates the study of the underlying mechanism[14]. Exploration of superconductivity at ambient pressure in the RP-phase $La_{n+1}Ni_nO_{3n+1}$

[1]Hefei National Research Center for Physical Sciences at the Microscale, University of Science and Technology of China, Hefei, Anhui, China. [2]Department of Physics, University of Science and Technology of China, Hefei, Anhui, China. [3]Shanghai Key Laboratory of Material Frontiers Research in Extreme Environments (MFree), Institute for Shanghai Advanced Research in Physical Sciences (SHARPS), Shanghai, China. [4]Center for High Pressure Science and Technology Advanced Research, Shanghai, China. [5]Information Materials and Intelligent Sensing Laboratory of Anhui Province, Anhui Key Laboratory of Magnetic Functional Materials and Devices, Institutes of Physical Science and Information Technology, Anhui University, Hefei, China. [6]Shanghai Synchrotron Radiation Facility, Shanghai Advanced Research Institute, Chinese Academy of Sciences, Shanghai, China. [7]Hefei National Laboratory, University of Science and Technology of China, Hefei, China. [8]Collaborative Innovation Center of Advanced Microstructures, Nanjing University, Nanjing, China. [9]These authors contributed equally: Mengzhu Shi, Di Peng. ✉e-mail: wutao@ustc.edu.cn; chenxh@ustc.edu.cn

not only offers a promising strategy to overcome the above challenges, but also has significant importance for the application of nickelate superconductors.

In $La_3Ni_2O_{7-\delta}$, the NiO_6 octahedra are tilted away from the longest axis at ambient pressure, resulting in an orthorhombic structure with space group of *Amam* (Fig. 1a) rather than a tetragonal structure with space group of *I4/mmm* (Fig. 1b). In the double-layer $La_3Ni_2O_{7-\delta}$ with *Amam* structure, the bond angle of Ni–O–Ni between adjacent NiO_6 octahedra is 168°. Earlier transport and spectroscopic measurements have revealed a density-wave transition around 150 K at ambient pressure[27–33]. A similar density-wave transition has also been observed in the trilayer nickelate $La_4Ni_3O_{10-\delta}$, in which an intertwined density wave with both charge and spin order is revealed (~136 K)[34]. As pressure increases, the unit cell volume shrinks significantly, making the tilted NiO_6 octahedra unstable. Recent X-ray diffraction (XRD) experiments under high pressure revealed that high pressure induces a structural transition from orthorhombic to tetragonal, and the pressure-induced superconductivity occurs in a tetragonal structure with *I4/mmm*[35–37]. In the *I4/mmm* structure, the bond angle of Ni–O–Ni between adjacent NiO_6 octahedra becomes 180°. In earlier theory, this change of the bond angle of Ni–O–Ni can significantly affect the interlayer coupling between NiO planes and is thought to be important for achieving the superconductivity under high pressure[9]. Therefore, stabilizing the tetragonal structure becomes a prerequisite for exploring nickelate superconductivity at ambient pressure. On the other hand, recent density functional theory (DFT) calculation also indicates that this change of the bond angle of Ni–O–Ni has no significant effect on the band structure, especially for the d_{z^2} orbital dominant band[38]. Following this line, the tetragonal structure is not crucial for superconductivity. Instead, the suppression of the density-wave transition in orthorhombic double-layer $La_3Ni_2O_{7-\delta}$ is important for achieving superconductivity at ambient pressure. In the present study, we successfully obtained the tetragonal structure with *I4/mmm* in $La_3Ni_2O_{7-\delta}$ single crystals at ambient pressure. Moreover, the superconducting structure in pressurized orthorhombic $La_3Ni_2O_{7-\delta}$ has been revisited. Our results indicate that a tetragonal structure is not a necessary condition for achieving superconductivity in $La_3Ni_2O_{7-\delta}$. The existence of spin-density-wave (SDW) order at ambient pressure seems more vital for pressure-induced superconductivity.

Results

Tetragonal $La_3Ni_2O_{7-\delta}$ at ambient pressure

The as-grown $La_3Ni_2O_{7-\delta}$ samples are obtained by utilizing the melt salt as the flux (see "Methods" section for details), which are crystallized into an *Amam* orthorhombic structure with noticeable oxygen defects and exhibit an insulating behavior (Supplementary Fig. 1). The recent multislice electron ptychography measurement indicates that the oxygen deficiency appears mainly at the inner apical oxygen sites and such a kind of oxygen defect makes the oxygen content in $La_3Ni_2O_{7-\delta}$ single crystal quite inhomogeneous[17]. After an additional post-annealing process under oxygen pressure of 10–15 bar to repair the oxygen defects, the temperature-dependent resistance becomes metallic while the orthorhombic structure is kept in $La_3Ni_2O_{7-\delta}$ samples (Fig. 1d and Supplementary Fig. 1). Pressure-induced high-temperature superconductivity can be observed in these annealed orthorhombic $La_3Ni_2O_{7-\delta}$ samples, which will be carefully discussed later. At this

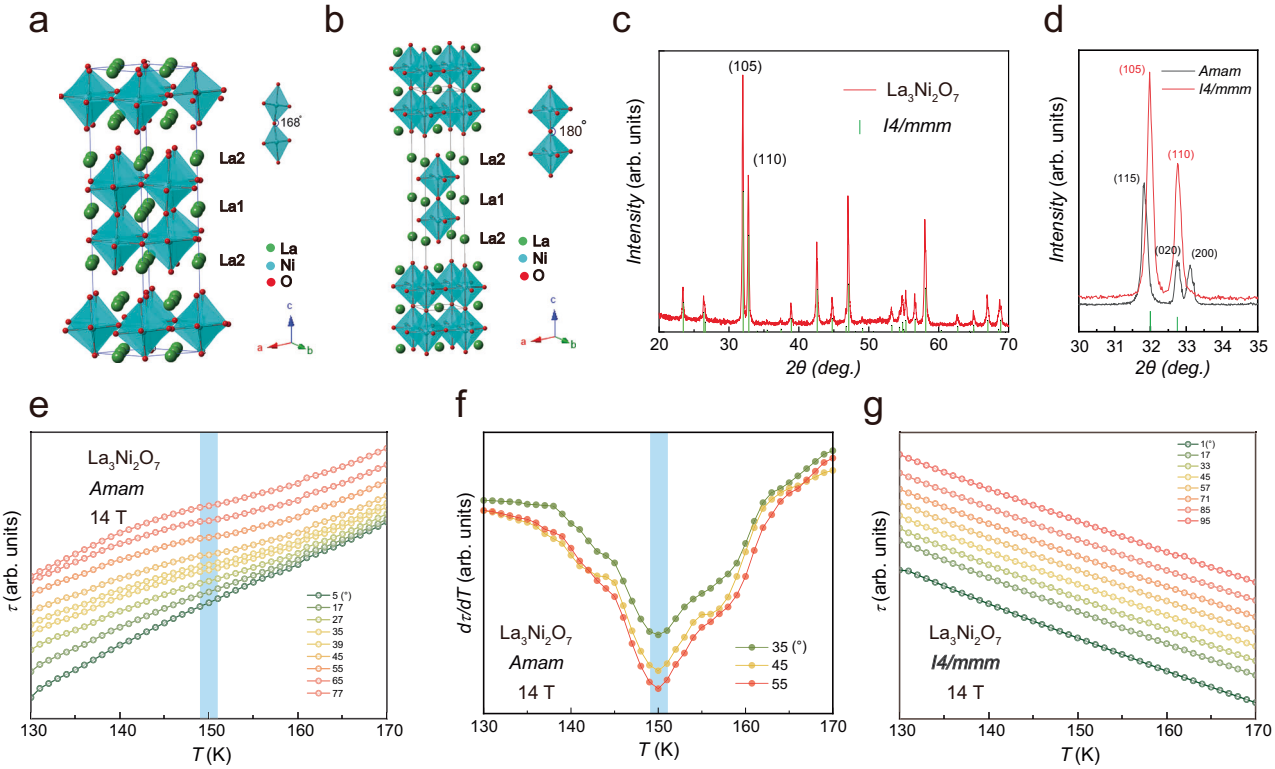

Fig. 1 | The structure and magnetic torque measurements for orthorhombic and tetragonal $La_3Ni_2O_{7-\delta}$ at ambient pressure. a and **b** The crystal structure model of orthorhombic and tetragonal $La_3Ni_2O_{7-\delta}$ at ambient pressure, respectively. There is a tilting angle between the adjacent NiO_6 octahedra for orthorhombic $La_3Ni_2O_{7-\delta}$, while the tilt along the c-axis disappears in the tetragonal $La_3Ni_2O_{7-\delta}$. **c** The powder XRD pattern for tetragonal $La_3Ni_2O_{7-\delta}$ at ambient pressure. **d** The enlarged XRD pattern between 30 and 35°, and the powder XRD pattern of the orthorhombic $La_3Ni_2O_{7-\delta}$ at ambient pressure are also plotted for comparison. **e** and **g** Temperature-dependent magnetic torque data of orthorhombic and tetragonal $La_3Ni_2O_{7-\delta}$, respectively. **f** Temperature-dependent $d\tau/dT$ at the angles of 35°, 45°, and 55°. There is an obvious feature in $\tau(T)$ around 150 K for orthorhombic $La_3Ni_2O_{7-\delta}$, implying the SDW transition, which is consistent with previous μSR and NMR results. Such a feature is not observed in the magnetic torque data for the tetragonal $La_3Ni_2O_{7-\delta}$, indicating no SDW transition for the tetragonal $La_3Ni_2O_{7-\delta}$.

https://doi.org/10.1038/s41467-025-63701-x

Table 1 | Crystal data and structure refinement for orthorhombic and tetragonal $La_3Ni_2O_{7-\delta}$ at ambient pressure

Identification code	$La_3Ni_2O_7$-OP	$La_3Ni_2O_7$-TP
Empirical formula	$La_3Ni_2O_{6.93}$	$La_3Ni_2O_{6.96}$
Formula weight	645.07	645.43
Temperature/K	299.6 (3)	301.70 (10)
Crystal system	orthorhombic	tetragonal
Space group	*Amam*	*I4/mmm*
a/Å	5.3908 (2)	3.8542 (2)
b/Å	5.4479 (2)	3.8542 (2)
c/Å	20.5353 (7)	20.2302 (18)
α/°	90	90
β/°	90	90
γ/°	90	90
Volume/Å^3	603.09 (4)	300.52 (4)
Z	4	2
ρ_{calc} g/cm^3	7.104	7.133
μ/mm^{-1}	167.489	168.076
F (000)	1130.0	565.0
Crystal size/mm^3	0.12 × 0.06 × 0.03	0.1 × 0.06 × 0.05
Radiation	Cu *Kα* (*λ* = 1.54184)	Cu *Kα* (*λ* = 1.54184)
2*Θ* range for data collection/°	8.612–156.138	8.742–153.538
Index ranges	$-6 \le h \le 6$, $-3 \le k \le 6$, $-25 \le l \le 25$	$-4 \le h \le 3$, $-4 \le k \le 4$, $-22 \le l \le 25$
Reflections collected	3006	1341
Independent reflections	373 [R_{int} = 0.0630, R_{sigma} = 0.0299]	128 [R_{int} = 0.0959, R_{sigma} = 0.0416]
Data/restraints/parameters	373/0/31	128/0/17
Goodness-of-fit on F^2	1.138	1.161
Final *R* indexes[$I >= 2\sigma(I)$]	*R*1 = 0.0374, *wR*2 = 0.1105	*R*1 = 0.0677, *wR*2 = 0.1733
Final *R* indexes [all data]	*R*1 = 0.0379, *wR*2 = 0.1110	*R*1 = 0.0678, *wR*2 = 0.1734
Largest diff. peak/hole/e Å^{-3}	1.97/−2.17	4.51/−5.35

stage, the oxygen content in orthorhombic $La_3Ni_2O_{7-\delta}$ is determined to be 6.85 by TG analysis (see Supplementary Fig. 2). With further increasing the annealing oxygen pressure to 150 bar, the orthorhombic structure is not stable anymore, and an *I4/mmm* tetragonal structure becomes stable in the $La_3Ni_2O_{7-\delta}$ single crystal. As shown in Fig. 1c, d, the powder XRD pattern of the tetragonal $La_3Ni_2O_{7-\delta}$, obtained by grinding several microcrystal pieces, can be well indexed by the calculated diffraction peaks for an *I4/mmm* tetragonal structure. As shown in Fig. 1d, the two peaks are well indexed as (105) and (110) in the tetragonal structure. No additional splitting due to orthorhombic distortion is observed in this range of 2*θ*. In comparison, obvious peak splitting can be observed for the orthorhombic $La_3Ni_2O_{7-\delta}$ as shown in Fig. 1d. In addition, the oxygen content in the tetragonal $La_3Ni_2O_{7-\delta}$ at ambient pressure is also determined by TG analysis (see Supplementary Fig.2 and Supplementary Table 1), and is about 6.92, slightly higher than that in orthorhombic $La_3Ni_2O_{6.85}$. Furthermore, the HAADF-STEM and iDPC data are also collected for tetragonal $La_3Ni_2O_{7-\delta}$ (see Supplementary Fig. 3). The tetragonal $La_3Ni_2O_{7-\delta}$ sample keeps a bi-layer RP structure without intergrowth with other RP phases (trilayer or perovskite phases). Moreover, there is no interstitial oxygen observed in the tetragonal $La_3Ni_2O_{7-\delta}$ sample.

In tetragonal $La_3Ni_2O_{6.92}$, the bond angles of Ni–O–Ni between adjacent NiO_6 octahedra along the longest axis change from 168° to 180°. Moreover, the in-plane Ni–O–Ni bonding angle at ambient pressure is 178.9°, which is quite consistent with the previously reported value of 178.4° for tetragonal $La_3Ni_2O_{7-\delta}$ under high pressure[35]. More detailed crystal data and refinement information are presented in Table 1 and Supplementary Fig.4.

It should be noted that no density-wave and no superconducting transition is observed in the temperature-dependent resistance of tetragonal $La_3Ni_2O_{7-\delta}$ at ambient pressure (Supplementary Fig. 1). This is one of the interesting findings in the present work. Since the signature of the density-wave transition is weak, and even no feature can be seen in resistance in orthorhombic $La_3Ni_2O_{7-\delta}$, we choose to utilize the magnetic torque technique to detect the possible density-wave transition in tetragonal $La_3Ni_2O_{7-\delta}$ at ambient pressure. First, we measure the magnetic torque in orthorhombic $La_3Ni_2O_{7-\delta}$ to make a benchmark for the SDW transition. As shown in Fig. 1e, the temperature-dependent magnetic torque $\tau(T)$ of the orthorhombic $La_3Ni_2O_{7-\delta}$ shows a clear *S*-shape behavior around 150 K, which is ascribed to the reported SDW transition by different techniques[29,31,32]. This SDW transition is more clearly seen in the $d\tau/dT$ vs T curves (Fig. 1f). Furthermore, as shown in Fig. 1g, the temperature-dependent $\tau(T)$ is also measured in the tetragonal $La_3Ni_2O_{7-\delta}$. In contrast to orthorhombic $La_3Ni_2O_{7-\delta}$, no SDW transition can be resolved in our present measurement. This result indicates that the SDW transition is absent in the tetragonal $La_3Ni_2O_{7-\delta}$. More implications of these results will be discussed later. Next, we will further explore the pressure-induced superconductivity in both orthorhombic and tetragonal $La_3Ni_2O_{7-\delta}$ samples.

Transport properties of pressurized orthorhombic and tetragonal $La_3Ni_2O_{7-\delta}$

To investigate the pressure-induced superconductivity in $La_3Ni_2O_{7-\delta}$ with different structures, we performed resistance measurements on selected microcrystals under high pressures. Helium gas was loaded as the pressure-transmitting medium to provide a homogeneous pressure environment[39]. The transport properties of the orthorhombic $La_3Ni_2O_{7-\delta}$ microcrystal under various pressures are shown in Fig. 2. In pressurized orthorhombic $La_3Ni_2O_{7-\delta}$, the room-temperature resistance gradually decreases with increasing pressure. At 15.3 GPa, the pressure-induced superconductivity appears in the temperature-dependent resistance, but the superconducting transition is still broad. By further increasing pressure, the superconducting transition becomes more pronounced, and a sharp superconducting transition can be achieved above 20 GPa, as shown in Fig. 2a, b. The highest onset temperature of the superconducting transition reaches to about 80 K while zero resistance temperature is about 45–43.5 K for two samples as shown in the inset of Fig. 2c and Supplementary Fig. 5a. These results on pressure-induced superconductivity are even better than the best superconducting transition in pressurized $La_3Ni_2O_{7-\delta}$ in reported literature[9,16], indicating the importance of the homogeneous pressure environment for the high-pressure measurements and the high quality of our annealed orthorhombic $La_3Ni_2O_{7-\delta}$ samples. By increasing the pressure above 20 GPa, the superconducting transition temperature starts to decrease slowly with increasing pressure, which is also consistent with previous high-pressure measurements[9,16]. The nature of optimal superconductivity is also examined by applying a magnetic field perpendicular to the Ni–O planes. As shown in Fig. 2c and Supplementary Fig. 5a, the superconducting transition under different magnetic fields is measured in two superconducting orthorhombic $La_3Ni_2O_{7-\delta}$ samples. The field-dependent superconducting transition temperatures are fitted by a Ginzburg–Landau (GL) model (Fig. 2d and Supplementary Fig. 5), and the extracted upper critical fields are comparable with the reported values in literature[9,16]. We note that there is a jump in the resistance curve recorded between 0 T and 0.1 T, which is possible due to the thermally activated flux flow[16].

https://doi.org/10.1038/s41467-025-63701-x

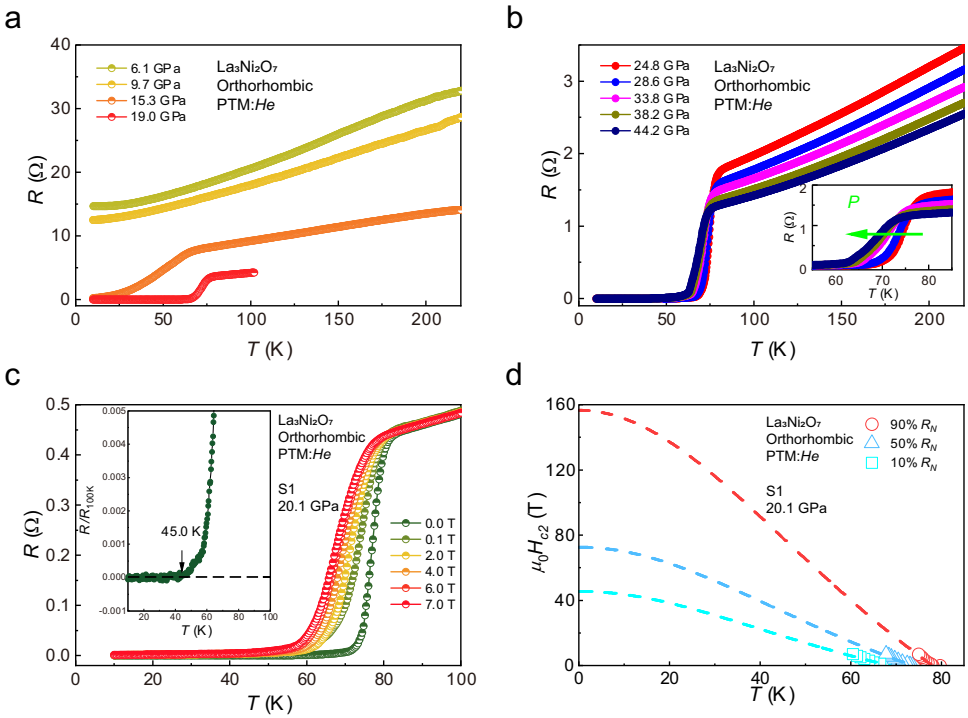

Fig. 2 | Temperature dependence of resistance (R) under various pressures for orthorhombic $La_3Ni_2O_{7-\delta}$. **a** and **b** Temperature-dependent resistance curves for the orthorhombic $La_3Ni_2O_{7-\delta}$ under different pressures. The inset of (b) shows the gradual suppression of T_c by pressure above 20 GPa. **c** The $R(T)$ curves for the orthorhombic $La_3Ni_2O_{7-\delta}$ under various magnetic field at 20.1 GPa. The superconducting transition is gradually suppressed to a low temperature with increasing magnetic field. The inset clearly shows that the temperature of zero resistance is as high as 45 K, which is the highest temperature of zero resistance reported in the $La_3Ni_2O_{7-\delta}$ single crystals so far. **d** The upper critical field for the orthorhombic $La_3Ni_2O_{7-\delta}$ sample is shown in (**c**). The upper critical fields were fitted with different criteria using a 3D GL model. In the 3D GL model, the H_c-T relation for a superconductor follows the equation $\mu_0 H_{c2}(T) = \mu_0 H_{c2}(0)\frac{1-(\frac{T}{T_c})^2}{1+(\frac{T}{T_c})^2}$ where H_{c2} and T_c are the upper critical field and superconducting temperature. As there is a jump in the resistance curves recorded at 0 T and 0.1 T in (**c**), the fitted upper critical field will be influenced by the criterion of the T_c defined. We show the fitting results of the upper critical field with different criteria of 10%, 50% and 90% R_N. There is a gap region between the red and cyan dotted lines, which indicates the thermally activated flux flow[16]. The positive curvature close to T_c in the low magnetic field region indicates the multi-band characteristic in nickelate superconductors under pressure.

In the case of tetragonal $La_3Ni_2O_{7-\delta}$, we first try to study the pressure effect on resistance by utilizing Helium gas as the pressure-transmitting medium. As shown in Fig. 3a, b, the temperature-dependent resistance shows the metallic behavior in the whole temperature range, and no significant pressure effect on the overall metallic behavior is observed with increasing pressure. Although the room-temperature resistance continuously decreases with increasing pressure, no superconductivity is observed up to 30.3 GPa. Then, we try to extend the study of pressure effect to higher pressure by utilizing NaCl as the pressure-transmitting medium. As shown in Fig. 3c, d, superconductivity is still absent up to 68.2 GPa. The fact that the metallic behavior without density-wave transition persists to high pressures indicates a robust ground state in tetragonal $La_3Ni_2O_{7-\delta}$, which is distinct from the pressurized orthorhombic $La_3Ni_2O_{7-\delta}$. On the other hand, the absence of superconductivity in pressurized tetragonal $La_3Ni_2O_{7-\delta}$ also poses a great challenge to the idea that the tetragonal structure is crucial for pressure-induced superconductivity. Next, we further study the high-pressure structure in orthorhombic and tetragonal $La_3Ni_2O_{7-\delta}$ to check the pressure-induced structural transition.

Structural evolution with pressure for the orthorhombic and tetragonal $La_3Ni_2O_{7-\delta}$

We conducted high-pressure powder XRD measurements on both orthorhombic and tetragonal $La_3Ni_2O_{7-\delta}$ samples by utilizing Helium gas as the pressure-transmitting medium, as illustrated in Fig. 4 and Supplementary Figs. 6–11. In principle, the helium pressure-transmitting medium offers a more homogeneous pressure environment compared to the previous measurements by utilizing liquid silicon oil as a transmitting medium[35–37]. In pressurized tetragonal $La_3Ni_2O_{7-\delta}$, the powder XRD data under different pressures are well fitted by a tetragonal structure with the space group of *I4/mmm* (see examples for 1.7 GPa and 21.7 GPa in Fig. 4b and Supplementary Fig. 6), and no peak splitting related to the orthorhombic distortion is resolved. As shown in Fig. 4c, the determined lattice parameters (*a*-axis and *c*-axis) and cell volume exhibit an almost linear decrease with increasing pressure, suggesting the absence of structural transition in tetragonal $La_3Ni_2O_{7-\delta}$ under pressure up to 31.3 GPa.

Similarly, our present work found that the orthorhombic $La_3Ni_2O_{7-\delta}$ also exhibits a stable orthorhombic structure up to 25.6 GPa as indicated by the powder XRD data (Fig. 4d, e). This result is quite different from the previous observation in orthorhombic $La_3Ni_2O_{7-\delta}$[35–37]. In detail, the splitting of the (020) and (200) peaks, attributed to orthorhombic distortion, is observed at all pressures (see examples for 1.5 GPa and 21.8 GPa in Fig. 4e and Supplementary Figs. 8 and 10). The derived lattice parameters and cell volume for orthorhombic $La_3Ni_2O_{7-\delta}$ are illustrated in Fig. 4f. It is obvious that the lattice parameters exhibit an almost linear decrease with increasing pressure, suggesting the absence of a structural transition under pressure. As shown in Supplementary Fig. 8, the powder XRD patterns for $La_3Ni_2O_{7-\delta}$ at 1.5 GPa and 21.8 GPa can be accurately fitted by the *Amam* space group. All these results strongly support that the pressure-induced superconducting phase remains in the orthorhombic structure. More detailed Ni–O bond lengths and Ni–O–Ni bond angles are shown in Supplementary Fig.11. We note that the bond length for the axial Ni–O (denoted as d_3 in

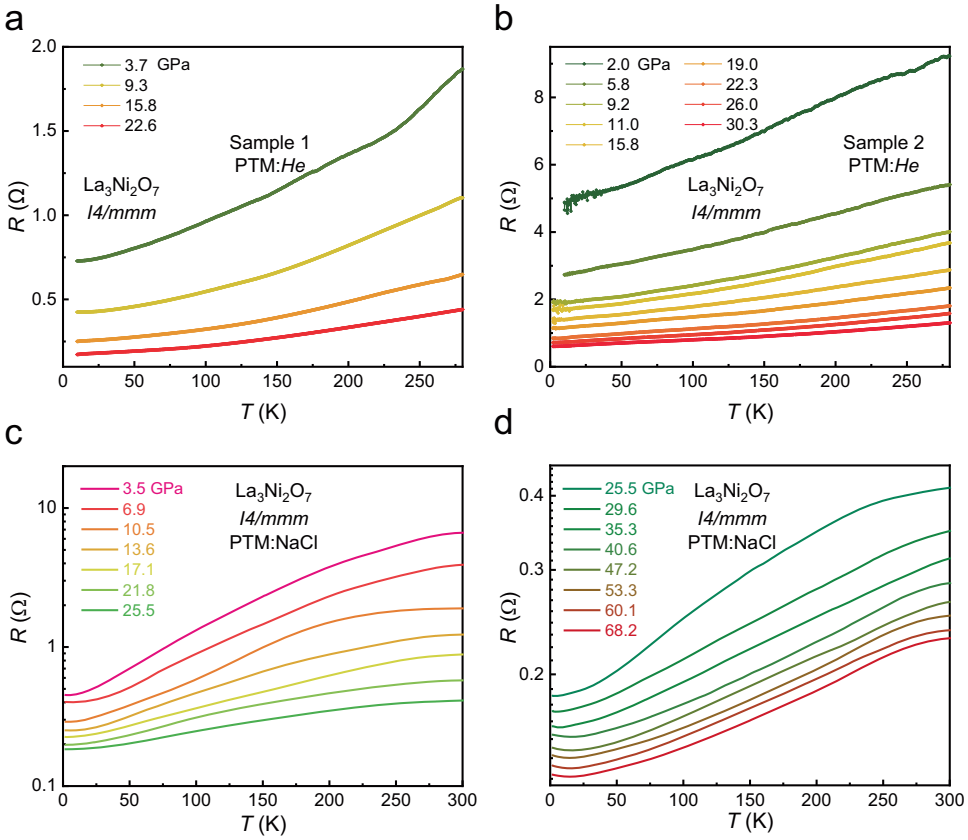

Fig. 3 | Temperature dependence of resistance (*R*) under various pressures for tetragonal $La_3Ni_2O_{7-\delta}$. **a** and **b** Temperature-dependent resistance for tetragonal $La_3Ni_2O_{7-\delta}$ under various pressures for two samples. The *R*(*T*) curves show a metallic behavior without any trace originating from superconducting transition or SDW under the pressure up to 30.3 GPa in the whole temperature range. All the above measurements were conducted on a DAC using Helium gas as the pressure-transmitting medium so as to get a more homogeneous pressure environment. **c** and **d** The *R*(*T*) curves for tetragonal $La_3Ni_2O_{7-\delta}$ at various pressures using NaCl as the pressure-transmitting medium. The resistance continually decreases with increasing pressure, and no anomaly arising from the superconductivity or SDW is observed. To compare the two different pressure-transmitting media, *R*(*T*) shows some difference due to pressure inhomogeneity, especially a slight upturn shows up at low temperature below 20 K under high pressure above 40 GPa for the case of using NaCl as the pressure-transmitting medium.

Supplementary Fig.11a) in *I4/mmm* phase $La_3Ni_2O_{7-\delta}$ is always ~0.15 Å shorter than that of *Amam* phase $La_3Ni_2O_{7-\delta}$ under the same pressure (see detail in Supplementary Fig. 11), which might influence the electronic structure and hence affect properties, including density wave(s) and superconductivity.

To compare with the reported literature, we conducted pressure-dependent powder XRD measurements on orthorhombic $La_3Ni_2O_{7-\delta}$ by utilizing silicon oil as the pressure-transmitting medium, which is a method commonly employed in prior studies[35–37]. As shown in Supplementary Fig. 12, the evolution of diffraction peaks (020) and (200) is quite consistent with previous reports and looks like gradually merging under pressure above 11 GPa. Considering the present results with Helium gas as the pressure-transmitting medium, this phenomenon is probably due to the inhomogeneity of the pressure environment, underscoring the importance of pressure homogeneity in high-pressure experiments. These results definitely indicate no pressure-induced structural transition in the orthorhombic $La_3Ni_2O_{7-\delta}$, and the structural transition reported previously could be ascribed to pressure inhomogeneity, which leads to the broadening of the diffraction peaks and causes the (020) and (200) diffraction peaks to merge together, consequently.

Discussion

Now we discuss the potential implications of the present work for exploring the RP-phase nickelate superconductors at ambient pressure. Previous studies have proposed that one of the key roles of high-pressure-induced superconductivity lies in stabilizing the tetragonal structure without octahedral tilting, as observed in both $La_3Ni_2O_{7-\delta}$ and $La_4Ni_3O_{10-\delta}$[11,35]. In fact, the role of the d_{z^2} orbital on the high-pressure superconductivity in $La_3Ni_2O_{7-\delta}$ and $La_4Ni_3O_{10-\delta}$ remains a subject of active debate[9,14]. Earlier theoretical proposals consider that the $3d_{z^2}$-derived bonding band below the Fermi energy will be lifted to form the γ pocket and plays a key role in the pressure-induced superconductivity, while the octahedral tilting is suppressed with increasing pressure[9,14]. This theoretical idea highlights the significance of synthesizing tetragonal $La_3Ni_2O_{7-\delta}$ and $La_4Ni_3O_{10-\delta}$ crystals for achieving superconductivity at ambient pressure. However, such a scenario is rather difficult to prove due to the limitations of experimental characterizations at high pressure. Moreover, the recent DFT calculation suggests that the $3d_{z^2}$-derived bonding band might not cross the Fermi level and plays a less significant role in the pressure-induced superconductivity[38]. Therefore, the successful growth of the tetragonal $La_3Ni_2O_{7-\delta}$ at ambient pressure in this work is quite important to solve the above argument.

It is well known that by significantly reducing the oxygen content, the tetragonal structure has been previously achieved at ambient pressure in $La_3Ni_2O_6$, where the apical oxygen atoms are completely removed[31]. However, in these oxygen-deficient tetragonal phases, no superconductivity has been reported, and they show an extremely insulating behavior[17,31]. This is significantly different from our

https://doi.org/10.1038/s41467-025-63701-x

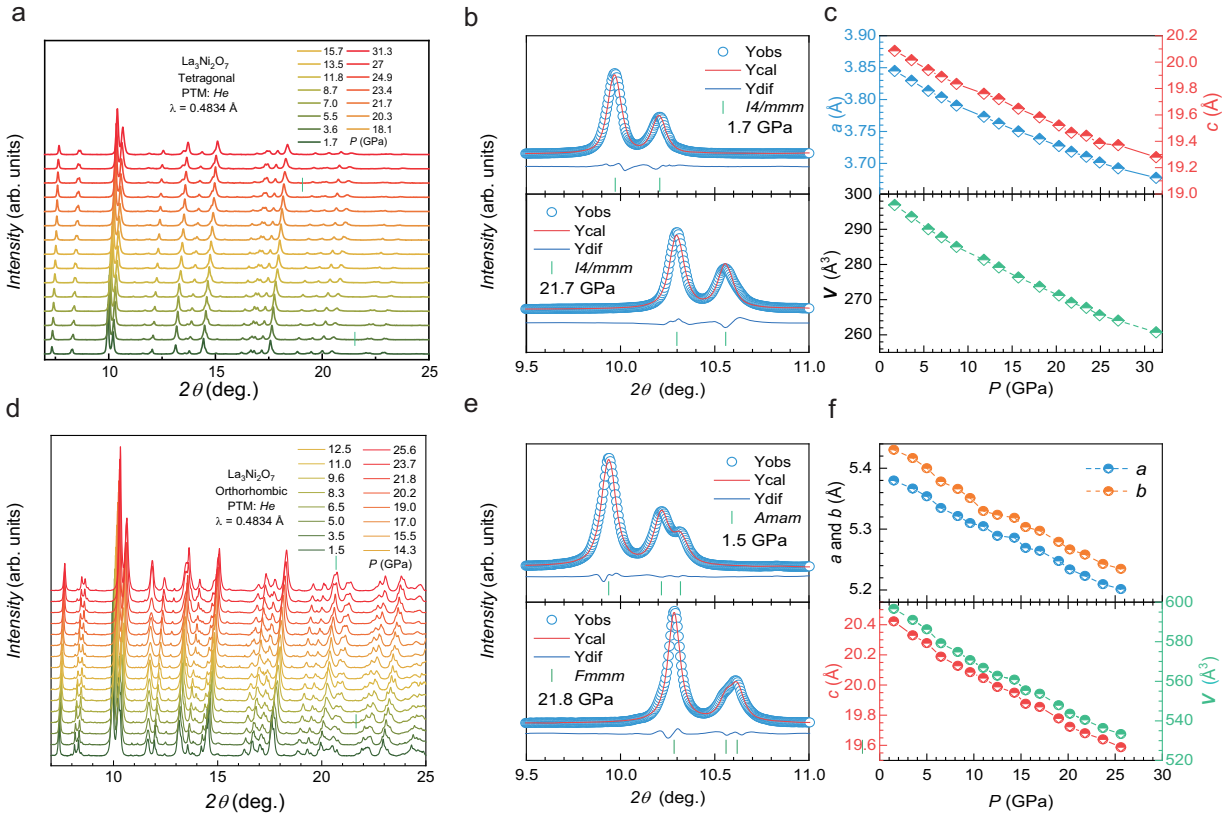

Fig. 4 | Evolution of X-ray diffraction patterns and lattice parameters with pressure for the tetragonal and orthorhombic $La_3Ni_2O_{7-\delta}$. **a** The powder XRD patterns for the tetragonal $La_3Ni_2O_{7-\delta}$ under different pressures. **b** Rietveld refinement of powder XRD patterns for the tetragonal $La_3Ni_2O_{7-\delta}$ under 1.7 GPa (the upper panel) and 21.7 GPa (the lower panel), respectively. The blue circles and red lines represent the observed and calculated data, respectively. The blue lines indicate the difference between the observed and calculated data. The short green vertical lines indicate the calculated diffraction peak positions. The powder XRD patterns can be well fitted with the space group *I4/mmm* at 2.5 GPa and 22.1 GPa. **c** The evolution of lattice parameters and cell volume with pressure for the tetragonal $La_3Ni_2O_{7-\delta}$. The blue and red dots are the lattice parameters for the *a*-axis and the *c*-axis, respectively. **d** The powder XRD patterns for the orthorhombic $La_3Ni_2O_{7-\delta}$ under different pressures. **e** Rietveld refinement of powder XRD patterns for the orthorhombic $La_3Ni_2O_{7-\delta}$ under 1.5 GPa (the upper panel) and 21.8 GPa (the lower panel) using the space group of *Amam*. Supplementary Fig. 9 shows the Rietveld refinement of the powder XRD pattern taken at 21.8 GPa using *Amam* and *Fmmm* as the space group. Both the *Amam* and *Fmmm* space groups fit well with the measured data, and we cannot determine its space group based on the current data. **f** The evolution of lattice parameters and cell volume with pressure for the orthorhombic $La_3Ni_2O_{7-\delta}$. The blue, orange, and red dots are the lattice parameters for the *c*-axis, *b*-axis, and *a*-axis, respectively. Helium gas was used as the pressure-transmitting medium during the measurement of all these powder XRD patterns so as to get a more homogeneous pressure environment.

tetragonal $La_3Ni_2O_{7-\delta}$ samples, which are annealed under a high-pressure oxygen atmosphere. Although precise determination of the oxygen content remains challenging due to the small sample size, the refinements of single crystal X-ray diffraction (SC-XRD) data on the crystal structure suggest an oxygen content very close to stoichiometry (see "Methods" section). In fact, the oxygen content of the tetragonal $La_3Ni_2O_{7-\delta}$ is found to be slightly higher than that of the orthorhombic $La_3Ni_2O_{7-\delta}$. Consequently, the absence of superconductivity in the tetragonal $La_3Ni_2O_{7-\delta}$ samples cannot be attributed to the oxygen defects. This conclusion is further supported by the metallic resistivity behavior as shown in Fig. 3. Moreover, our high-pressure XRD measurements on the orthorhombic $La_3Ni_2O_{7-\delta}$ samples reveal that the structure of the high-pressure superconducting phase is orthorhombic rather than tetragonal, in stark contrast with previous studies[35]. It should be emphasized that the hydrostatic pressure is highly desirable to detect such tiny differences in different structures under high pressures, which highlights the importance of hydrostatic conditions in high-pressure work. All these findings challenge the idea that high-pressure superconductivity emerges upon the formation of a tetragonal structure, and suggest that a tetragonal structure is not a necessary condition for achieving superconductivity in double-layer $La_3Ni_2O_{7-\delta}$. On the other hand, recent studies have confirmed SDW order in orthorhombic $La_3Ni_2O_{7-\delta}$ using various spectroscopic probes, including resonant inelastic X-ray scattering (RIXS)[40], nuclear magnetic resonance (NMR)[32], and muon spin rotation (μSR) experiments[29,41]. However, our transport and magnetic torque measurements reveal no evidence of any SDW transitions in the tetragonal $La_3Ni_2O_{7-\delta}$. Together with the absence of superconductivity, it implies that the SDW transition, rather than the tetragonal symmetry, is the primary condition for the pressure-induced superconductivity. By further analyzing the average in-plane lattice ($a_p = \sqrt{a^2 + b^2}$) and the ratio of c/a_p, we found that, although the value of a_p in the whole pressure range is comparable in both tetragonal and orthorhombic $La_3Ni_2O_{7-\delta}$, the value of c/a_p in tetragonal $La_3Ni_2O_{7-\delta}$ is smaller than that in orthorhombic $La_3Ni_2O_{7-\delta}$ (see Supplementary Fig.13). This means that the absence of SDW transition and superconductivity in tetragonal $La_3Ni_2O_{7-\delta}$ might be related to the effect of c/a_p on the underlying electronic structure. Further experimental investigation on the tetragonal $La_3Ni_2O_{7-\delta}$ at ambient pressure is needed to understand the deep correlation between SDW order and superconductivity in double-layer $La_3Ni_2O_{7-\delta}$. Our finding that the structure type and SDW order in double-layer $La_3Ni_2O_{7-\delta}$ strongly depend on the oxygen concentration paves the way to explore high-T_c superconductivity at ambient pressure in nickelate superconductors.

Methods

Sample growth

The $La_3Ni_2O_{7-\delta}$ crystals are grown through a melt salt method. Firstly, the Lanthanum nitrate hexahydrate, nickel (II) nitrate hexahydrate and citric acid (CA) were dissolved in the water with the mole ratio CA: La: Ni = 5:3:2. After preheated at 140 °C in an oven for about 24 h, the above product was transferred into a muffle furnace where the temperature is slowly increased to 400 °C in 10 h and kept for another 10 h. The above precursor (P) is mixed with a salt flux (NaCl/KCl mixture) at the mass ratio of P: NaCl: KCl = 1:14:16 and loaded into a corundum crucible. The corundum crucible is heated in the air to 1150 °C in 10 h and kept for 48 h, and then slowly cooled down to 1110 °C in 7 days. A microcrystal with a typical size of 0.1 × 0.1 × 0.03 mm was obtained after washing the flux using water. The as-grown product is orthorhombic $La_3Ni_2O_{7-\delta}$ with an insulating behavior due to oxygen deficiency. Then the microcrystals are annealed at high oxygen pressure to obtain metallic $La_3Ni_2O_{7-\delta}$. The annealing temperature is slowly increased to 500 °C in 10 h and kept for 5 h, then slowly cooled down to 50 °C in 6 days. For metallic orthorhombic $La_3Ni_2O_{7-\delta}$, the sample is annealed at 10–15 bar oxygen. For metallic tetragonal $La_3Ni_2O_{7-\delta}$, the sample is annealed at 150 bar oxygen. The refined oxygen content for the metallic sample based on the single crystal X-ray diffraction (SC-XRD) data is 6.932 ± 0.004 for the orthorhombic phase and 6.956 ± 0.0011 for the tetragonal phase, respectively. As the X-ray diffraction is not expected to be sensitive to light elements, the oxygen contents for both samples are measured using TG analysis, which is useful to determine the average oxygen content in the powder sample with higher sensitivity.

Ambient-pressure structural, composition, and magnetic torque characterization

The single crystal X-ray diffraction (SC-XRD) data was collected on a four-circle diffractometer (Rigaku, XtaLAB PRO 007HF) with Cu Kα radiation in the Core Facility Center for Life Sciences, USTC. The structure was solved and refined using Olex-2 with ShelXT and ShelXL packages. The detailed structure data is shown in Table 1. The powder XRD data at ambient pressure is collected at the SmartLab diffractometer equipped with the Cu target. The cross-sectional TEM sample of *I4/mmm* $La_3Ni_2O_{7-\delta}$ was prepared on a Carl Zeiss Crossbeam 550L FIB-SEM. The high-angle annular dark-field scanning transmission electron microscopy (HAADF-STEM) image and integrated differential phase contrast (iDPC) data are collected on a Thermo Fischer Scientific Titan Themis Z microscope operating at 300 kV. Thermogravimetric (TG) analysis for $La_3Ni_2O_{7-\delta}$ under the reduced environment (10% H_2 + 90%Ar) is conducted to calculate the oxygen content. Typically, a mass of ~200 mg sample is loaded on a TG balance (Nangjing Dazhan, DZ-STA200, accuracy of 0.01 mg). The calculated oxygen content is 6.85 and 6.92 for the sample annealed at 15 bar and 150 bar oxygen, respectively. More results are shown in Supplementary Fig.2 and the Supplementary Table 1.

Torque magnetometry was conducted in a Physical Properties Measurement System (PPMS, Quantum Design Inc., DynaCool-14T) using an SCL piezoresistive cantilever. The sample was attached to the tip of the cantilever, which was fixed on a horizontal rotator. We first rotated the sample in a range of θ (the angle between the magnetic field vector H and the flat plane of $La_3Ni_2O_{7-\delta}$ crystal) from 0° to 90° under isothermal conditions and determined that the largest signal occurs at approximately θ close to 45°.

High-pressure electrical transport and XRD measurements

The high-pressure resistance for $La_3Ni_2O_{7-\delta}$ single crystals was measured in the diamond anvil cells by using NaCl or Helium gas as the pressure-transmitting medium. Diamond anvils with various culets (200–400 μm) were used for high-pressure transport measurements. The pressure was applied and calibrated by the shift of ruby fluorescence at room temperature. The transport measurements were carried out in a refrigerator system (HelioxVT, Oxford Instruments) or Physical Properties Measurement System (PPMS-9, Quantum Design Inc.). The powder XRD data of tetragonal and orthorhombic $La_3Ni_2O_{7-\delta}$ under pressure is collected at Shanghai Synchrotron Radiation Facility, using an X-ray beam with a wavelength of 0.4834 Å. The Helium gas or silicon oil was used as the pressure-transmitting medium for orthorhombic $La_3Ni_2O_{7-\delta}$. Two-dimensional diffraction images were recorded by a PILATUS R CdTe detector and subsequently processed into one-dimensional XRD patterns using the Dioptas software. The powder XRD data were refined using the Jana2020 or GSAS-II software to obtain the lattice parameters under different pressures.

Data availability

The experimental data presented in the main text figures have been deposited in the figshare database under accession code https://doi.org/10.6084/m9.figshare.29626373. The detailed crystal structure data in this study have been deposited in the Cambridge Crystallographic Data Centre (CCDC) website with the deposition numbers CSD 2474658 and 2474696. The data that support the findings of this study are available from the corresponding author upon request.

Code availability

The code that supports the findings of this study is available from the corresponding author upon request.

References

1. Bednorz, J. G. & Müller, K. A. Possible high T_c superconductivity in the Ba–La–Cu–O system. *Z. Phys. B Condens. Matter* **64**, 189–193 (1986).
2. Norman, M. R. Materials design for new superconductors. *Rep. Prog. Phys.* **79**, 074502 (2016).
3. Azuma, M., Hiroi, Z., Takano, M., Bando, Y. & Takeda, Y. Superconductivity at 110 K in the infinite-layer compound $(Sr_{1-x}Ca_x)_{1-y}CuO_2$. *Nature* **356**, 775–776 (1992).
4. Anisimov, V. I., Bukhvalov, D. & Rice, T. M. Electronic structure of possible nickelate analogs to the cuprates. *Phys. Rev. B* **59**, 7901–7906 (1999).
5. Lee, K.-W. & Pickett, W. E. Infinite-layer $LaNiO_2$: Ni^{1+} is not Cu^{2+}. *Phys. Rev. B* **70**, 165109 (2004).
6. Crespin, M., Levitz, P. & Gatineau, L. Reduced forms of $LaNiO_3$ perovskite. Part 1.—Evidence for new phases: $La_2Ni_2O_5$ and $LaNiO_2$. *J. Chem. Soc. Faraday Trans. 2* **79**, 1181–1194 (1983).
7. Hayward, M. A., Green, M. A., Rosseinsky, M. J. & Sloan, J. Sodium hydride as a powerful reducing agent for topotactic oxide deintercalation: synthesis and characterization of the nickel(I) oxide $LaNiO_2$. *J. Am. Chem. Soc.* **121**, 8843–8854 (1999).
8. Li, D. et al. Superconductivity in an infinite-layer nickelate. *Nature* **572**, 624–627 (2019).
9. Sun, H. et al. Signatures of superconductivity near 80 K in a nickelate under high pressure. *Nature* **621**, 493–498 (2023).
10. Li, Q. et al. Signature of superconductivity in pressurized $La_4Ni_3O_{10}$. *Chin. Phys. Lett.* **41**, 017401 (2024).
11. Zhu, Y. et al. Superconductivity in tri-layer nickelate $La_4Ni_3O_{10}$ single crystals. *Nature* **631**, 531–536 (2024).
12. Zhang, M. et al. Superconductivity in tri-layer nickelate $La_4Ni_3O_{10}$ under pressure. *Phys. Rev. X* **15**, 021005 (2025).
13. Sakakibara, H. et al. Theoretical analysis on the possibility of superconductivity in the tri-layer Ruddlesden-Popper nickelate $La_4Ni_3O_{10}$ under pressure and its experimental examination: Comparison with $La_3Ni_2O_7$. *Phys. Rev. B* **109**, 144511 (2024).
14. Wang, M., Wen, H.-H., Wu, T., Yao, D.-X. & Xiang, T. Normal and superconducting properties of $La_3Ni_2O_7$. *Chin. Phys. Lett.* **41**, 077402 (2024).

15. Yang, J. et al. Orbital-dependent electron correlation in double-layer nickelate $La_3Ni_2O_7$. *Nat. Commun.* **15**, 4373 (2024).
16. Zhang, Y. et al. High-temperature superconductivity with zero resistance and strange-metal behavior in $La_3Ni_2O_{7-\delta}$. *Nat. Phys.* **20**, 1269–1273 (2024).
17. Dong, Z. et al. Visualization of oxygen vacancies and self-doped ligand holes in $La_3Ni_2O_{7-\delta}$. *Nature* **630**, 847–852 (2024).
18. Wang, G. et al. Pressure-induced superconductivity in polycrystalline $La_3Ni_2O_{7-\delta}$. *Phys. Rev. X* **14**, 011040 (2024).
19. Puphal, P. et al. Unconventional crystal structure of the high-pressure superconductor $La_3Ni_2O_7$. *Phys. Rev. Lett.* **133**, 146002 (2024).
20. Zhou, Y. G. et al. Investigations of key issues on the reproducibility of high-Tc superconductivity emerging from compressed $La_3Ni_2O_{7-\delta}$. *Matter Radiat. Extremes* **10**, 027801 (2025).
21. Chen, X. et al. Polymorphism in the Ruddlesden–Popper nickelate $La_3Ni_2O_7$: discovery of a hidden phase with distinctive layer stacking. *J. Am. Chem. Soc.* **146**, 3640–3645 (2024).
22. Luo, Z., Hu, X., Wang, M., Wú, W. & Yao, D.-X. Bilayer two-orbital model of $La_3Ni_2O_7$ under pressure. *Phys. Rev. Lett.* **131**, 126001 (2023).
23. Christiansson, V., Petocchi, F. & Werner, P. Correlated electronic structure of $La_3Ni_2O_7$ under pressure. *Phys. Rev. Lett.* **131**, 206501 (2023).
24. Liu, Y. B., Mei, J. W., Ye, F., Chen, W. Q. & Yang, F. s± wave pairing and the destructive role of apical-oxygen deficiencies in $La_3Ni_2O_7$ under pressure. *Phys. Rev. Lett.* **131**, 236002 (2023).
25. Qu, X. Z. et al. Bilayer model and magnetically mediated pairing in the pressurized nickelate. *Phys. Rev. Lett.* **132**, 036502 (2024).
26. Zhang, Y., Lin, L. F., Moreo, A., Maier, T. A. & Dagotto, E. Structural phase transition, $s^{\pm}$-wave pairing, and magnetic stripe order in bilayered superconductor $La_3Ni_2O_7$ under pressure. *Nat. Commun.* **15**, 2470 (2024).
27. Sreedhar, K. et al. Low-temperature electronic properties of the $La_{n+1}Ni_nO_{3n+1}$ (n = 2, 3, and ∞) system: evidence for a crossover from fluctuating-valence to Fermi-liquid-like behavior. *J. Solid State Chem.* **110**, 208–215 (1994).
28. Zhang, Z., Greenblatt, M. & Goodenough, J. B. Synthesis, structure, and properties of the layered perovskite $La_3Ni_2O_{7-\delta}$. *J. Solid State Chem.* **108**, 402–409 (1994).
29. Chen, K. et al. Evidence of spin density waves in $La_3Ni_2O_{7-\delta}$. *Phys. Rev. Lett.* **132**, 256503 (2024).
30. Fukamachi, T., Kobayashi, Y., Miyashita, T. & Sato, M. 139 La NMR studies of layered perovskite systems $La_3Ni_2O_{7-\delta}$ and $La_4Ni_3O_{10}$. *J. Phys. Chem. Solids* **62**, 195–198 (2001).
31. Liu, Z. et al. Evidence for charge and spin density waves in single crystals of $La_3Ni_2O_7$ and $La_3Ni_2O_6$. *Sci. China Phys. Mech. Astron.* **66**, 217411 (2022).
32. Zhao, D. et al. Spin-density-wave transition in double-layer nickelate $La_3Ni_2O_7$. *Sci. Bull.* **70**, 1239–1245 (2025).
33. Kobayashi, Y. et al. Transport and magnetic properties of $La_3Ni_2O_{7-\delta}$ and $La_4Ni_3O_{10-\delta}$. *J. Phys. Soc. Jpn* **65**, 3978–3982 (1996).
34. Zhang, J. et al. Intertwined density waves in a metallic nickelate. *Nat. Commun.* **11**, 6003 (2020).
35. Wang, L. et al. Structure responsible for the superconducting state in $La_3Ni_2O_7$ at high pressure and low temperature conditions. *J. Am. Chem. Soc.* **146**, 7506–7514 (2024).
36. Wang, G. et al. Pressure-induced superconductivity in polycrystalline $La_3Ni_{2O7-\delta}$. *Phys. Rev. X* **14**, 011040 (2024).
37. Wang, N. et al. Bulk high-temperature superconductivity in pressurized tetragonal $La_2PrNi_2O_7$. *Nature* **634**, 579–584 (2024).
38. Wang, Y., Jiang, K., Wang, Z., Zhang, F.-C. & Hu, J. Electronic and magnetic structures of bilayer $La_3Ni_2O_7$ at ambient pressure. *Phys. Rev. B* **110**, 205122 (2024).
39. Klotz, S., Chervin, J. C., Munsch, P. & Le Marchand, G. Hydrostatic limits of 11 pressure transmitting media. *J. Phys. D Appl. Phys.* **42**, 075413 (2009).
40. Chen, X. et al. Electronic and magnetic excitations in $La_3Ni_2O_7$. *Nat. Commun.* **15**, 9597 (2024).
41. Khasanov, R. et al. Pressure-induced split of the density wave transitions in $La_3Ni_2O_{7-\delta}$. *Nat. Phys.* **21**, 430–436 (2025).

Acknowledgements

We acknowledge fruitful discussions with Ho-kwang Mao, Zhenyu Wang, and Ziji Xiang. We also thank Zhongliang Zhu, Xiaodong Li, Fei Zhang, Fujun Lan, Yuxin Liu, and Hongbo Lou for their experimental assistance. This work is supported by the National Natural Science Foundation of China (Grants No. 12494592) (to M.S. and J.Y.), 12488201 (to X.C.), 11888101 (to X.C.), 12034004 (to T.W.), 12161160316 (to T.W.), 12325403 (to T.W.), the National Key R&D Program of the MOST of China (Grant No. 2022YFA1602601) (to X.C. and T.W.), the Chinese Academy of Sciences under contract No. JZHKYPT-2021-08 (to X.C., T.W., and J.Y.), the CAS Project for Young Scientists in Basic Research (Grant No. YBR-048) (to J.Y., T.W., and M.S.), and the Innovation Program for Quantum Science and Technology (Grant No. 2021ZD0302802) (to T.W., J.Y., and X.C.). D.P. and Q.Z. acknowledge the financial support from the Shanghai Science and Technology Committee (Grant No. 22JC1410300) (to Q.Z. and D.P.) and Shanghai Key Laboratory of Material Frontiers Research in Extreme Environments (Grant No.22dz2260800) (to Q.Z. and D.P.). A portion of this research used resources at the beamline 17UM of Shanghai synchrotron radiation facility (https://cstr.cn/31124.02.SSRF.BL17UM) and the ID31-High Pressure Beamline of High Energy Photon Source (https://cstr.cn/31138.02.HEPS).

Author contributions

X.H.C. conceived the research project. X.H.C. and T.W. coordinated the experiments. M.Z.S. grew the single crystals and performed the structural characterization at ambient pressure; H.P.L. and K.B.F. measured the magnetic torque data; S.H.Y. and B.H.G. performed the TEM characterizations. Y.K.L., R.Q.W., and J.J.Y. performed the high-pressure transport measurement using NaCl as the pressure-transmitting medium; D.P. performed the resistance measurements using helium as a pressure-transmitting medium under pressure with the help of Q.S.Z.; D.P., Z.F.X., and Y.Z.W. performed the synchrotron powder diffraction measurements and analysis under high-pressure using helium and silicon oil as the pressure-transmitting medium with help from Q.S.Z. and Z.D.Z.; M.Z.S., D.P., J.J.Y., T.W., and X.H.C. analyzed the data; M.Z.S., D.P., J.J.Y., T.W., and X.H.C. wrote the paper with inputs from all authors.

Competing interests

The authors declare no competing interests.

Additional information

Supplementary information The online version contains supplementary material available at https://doi.org/10.1038/s41467-025-63701-x.

Correspondence and requests for materials should be addressed to Tao Wu or Xianhui Chen.

Peer review information *Nature Communications* thanks Jinguang Cheng and the other anonymous reviewer(s) for their contribution to the peer review of this work. A peer review file is available.